UNIVERSITY OF CALIFORNIA
UCO/LICK OBSERVATORY TECHNICAL REPORT
NO. 59

FINITE ELEMENT ANALYSIS OF LARGE LENSES FOR THE KECK TELESCOPE HIGH RESOLUTION ECHELLE SPECTROGRAPH

BRUCE BIGELOW

Santa Cruz, California
July 1992

Finite element analysis of large lenses for the Keck Telescope High Resolution Echelle Spectrograph

B. C. Bigelow

University of California Observatories/Lick Observatory
University of California, Santa Cruz, CA 95064

UCO/Lick Observatory Technical Report No. 59

ABSTRACT

The finite element analyses of two large lenses for the Keck Telescope High Resolution Echelle Spectrograph are described. The two lenses, one simple lens, and one meniscus, are of fused silica and are approximately 800 mm (30 in.) in diameter. The purpose of the analyses is to determine the deformations of each optic under its own weight, and to identify the simplest, most cost effective mounting cell that will satisfy the optical requirements. Two common radial supports are analyzed, including varieties of hard point and band type mountings. Several types of axial supports are examined including simple three-point mounts, ring mounts, and static deformation mounts. A parametric finite element input routine is described, whereby a solid model and finite element mesh are automatically generated, given the lens diameter, central thickness, and surface radii of curvature. Deformation predictions from the models are compared with theoretical calculations, interferometric testing, and precision profilometry.

1. INTRODUCTION

Optical instruments for large aperture telescopes have created a new need for large refracting optics. The optical design of instruments such as the Keck Telescope High Resolution Echelle Spectrograph (HIRES) calls for large lenses with high aspect ratios, light weight, and good transmissive performance. The combination of large diameters and narrow cross sections provides new challenges for mounting lenses for minimum elastic deformation under gravity. Two such lenses are analyzed here for elastic deformation due to weight and various distributed support systems. A variety of radial and axial supports are examined, including hard points, band mounts, and a static deformation mount. Models are generated and solutions are performed on a Sun® 4/110 using the ANSYS® finite element analysis package. Results from the finite element analyses are compared with theoretical calculations, interferometric, and profilometric tests of a subscale lens and a full size lens blank.

2. OPTICS AND MODELS

The two lenses are shown in **figure 1.** The first lens (C1) is a convex/concave meniscus with spherical surfaces, 770 mm (30.3 in.) in diameter, 25.4 mm (1 in.) thick at the center, an average aspect ratio of 9:1, and weighs 57 kg (126 lbs). The second lens (C2) is a simple biconvex element with spherical surfaces, 813 mm (32 in.) in diameter, 73 mm (2.87 in.) thick at the center, an average aspect ratio of 16:1, and weighs 53 kg (116 lbs). The lenses are oriented with their optical axes tilted 10.3 degrees from horizontal. Both lenses are made of Corning® 7940 fused silica, with elastic modulus of 73,081 MPa (10.6 E6 Psi), density of 2.202 gm/cm^3 (0.0796 lb/in.^{3}), and Poisson's ratio of 0.17.

A parametric model, as defined here, is a model whose configuration can quickly be modified by changing a small number of variables, or parameters. This feature vastly reduces the time required to perform a finite element analysis on a wide variety of optical shapes, because the solid model generation, which commonly requires more than half of the analyst's time, is done automatically. A general input file is used with data sections for lens parameters (diameter, center thickness, and radii of curvature), lens material properties (elastic modulus, density, and Poisson's ratio), mesh density parameters (axial, radial and thickness), and subroutine calls for radial and axial supports (hard point, band mount, ring mount, etc). Consequently, preprocessing (preparation of the solid and finite element models) is done by the computer, and requires only a quick check before running the solution phase. It should be noted that these analyses are all based on half geometry models, which are consequently limited to symmetric loading conditions. Since all the support types considered are symmetric, the half model is sufficient and greatly reduces solution time.

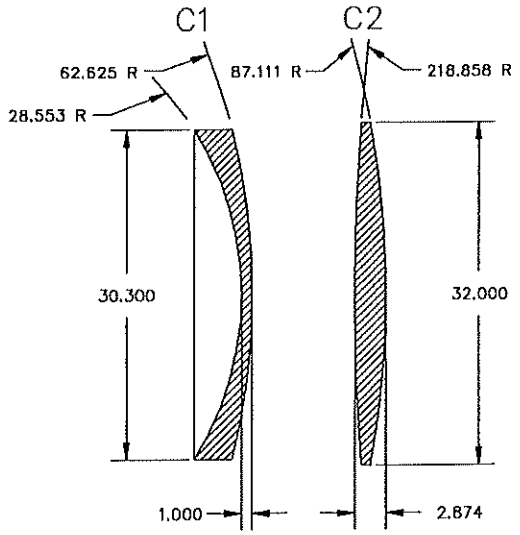

FIGURE 1. HIRES LENSES

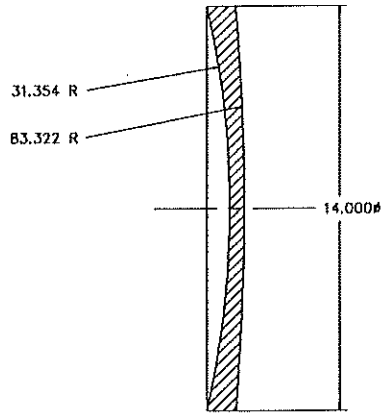

FIGURE 2. 14" TEST LENS

The parametric input routine is organized in three major sections. The first section contains data blocks for the physical dimensions of the lens, the material properties, and parameters for defining the mesh density in the radial, axial, and thickness directions.

The second section uses values from the data blocks to create the solid model geometry and the finite element mesh. By combining different values of positive and negative radii of curvature, the full range of biconvex, convex/concave, and biconcave lens type can be modeled. By providing very large values for one or both surface radii, any combination of curved and plano lenses can be produced. The input routine is able to produce all these varieties by defining the two optical surfaces as parts of two spherical coordinate systems (CS), separated by the appropriate radii and center thickness. Once the front and rear surfaces are defined, a third cylindrical coordinate system is defined, with its central axis laying between the centers of the two spherical coordinate systems. With the three CS's in place, the program proceeds to build a wire frame and solid model from points, lines, and surfaces. When all the surfaces are defined by wireframe lines, values from the mesh density data block are used to divide the lines into sections corresponding to the number of elements desired in each coordinate direction. The program then meshes the solid model with nodes and elements and assigns the appropriate material properties.

The third section of the input routine defines the boundary conditions for the various types of radial and axial support. Short subroutines are written and then recalled by the input program to apply forces, pressures, and moments as required for a given analysis. For radial support, the four types of boundary condition (BC) sets available for modeling are hard points, constant pressure (band or sling mount), variable pressure (mercury belt), and continuous (potted in elastomer). The mercury belt and potted support were not considered for this application and are not discussed. Axial supports are modeled by several variations on hard points, from a simple three point arrangement, to ring and whiffletree type mounts. Radial supports are described first, followed by axial supports.

For hard point supports, constraints are applied radially to nodes around the edge of the part. It is desirable to apply the radial constraints through the plane of the center of gravity (CG), to avoid creating an overturning moment in the optic. It is also generally preferable to split the support points into at least two contact points to reduce local stress and deformation.[1] The input routine reads the angle between hard points as a parameter, and the program searches for nodes at the CG plane and applies the constraints to the requested number of nodes.

For a band or sling type mount, the boundary conditions are assumed to be a constant pressure applied over a given angle to represent the wrap angle of the band.[2] If constant tension is assumed in the band, it can be shown that the band or sling will produce a constant pressure on the optic. With this assumption, the program calculates a pressure value, given the weight of the part and the width of the band, and applies it over an area centered on the CG of the optic. In all cases analyzed

here, a 180° wrap angle is used. Additionally, one node at the bottom of the optic is constrained to check that the pressure is correct. A very small reaction force at the constrained node indicates a correct pressure calculation.

The simplest axial support is modeled by three hard points spaced 120 degrees around the front of an optic. This can be expanded to two "split" or "whiffled" points, for a total of six, and then split again any number of times. Typically, the defining points are located in an annulus bordered by the outside edge of the optic and the edge of the clear aperture required.

A second, more complicated variation on hard points is considered here, and called a "static deformation mount." In this case, constraints are applied around the back surface of the optic, and forces are applied in a ring around the front surface. By varying the forces and the number of points of application, the optic can be statically deformed to counter the deformation due to gravity. In these analyses, the location and magnitude of forces varies among models. However, the varying of forces as a function of location in a given model is not examined.

3. CALIBRATION OF MODELS

The objective of the HIRES lens analyses is to find the simplest method of support which will give a maximum peak-to-valley (P-V) surface deformation of less than $\lambda/4$. In order to build confidence in the accuracy of the modeling process at the $\lambda/4$ (0.15 μm or 6 μin) level, a 355.6 mm (14 in.) diameter, fused silica concave/convex meniscus (**figure 2**) was analyzed under the same types of mountings and tested. Additionally, the blank for the simple lens was analyzed and tested under two types of axial mounts in the horizontal position. The results of the calibration analyses and tests for the 14 in. optic will be discussed first, followed by results from the lens blank.

3.1. 14 in. lens tests

The 14 in. optic is not a perfect analog for either of the larger lenses, but it was the largest element available for testing and, hopefully, would provide a good half-scale check on the finite element predictions. Previous interferometric tests indicated that the lens had a figure of $\lambda/18$, thought to be good enough for comparison testing. The order of analyses starts with variations on three simple "arc-stop" or hard point radial supports, and three axial supports, followed by variations on the band mount.

3.1.1. Hard point mount tests

The parametric input file was used to produce the FEA model with the following values: Dia. = 355.6 mm (14 in.), R1 = 798.8 mm (31.4 in.), R2 = 2092.1 mm (82.3 in.), and axial thickness 12.57 mm (0.50 in.). The mesh parameters created a model with 790 nodes and 552 elements (**figure 3**). The analyses were run with the optical axis of the part horizontal. Ten analyses were run with the angle between the radial points at 0°, 30°, 60°, 90°, and 120°. For each angle, two radial support trials were run, one with only individual CG nodes constrained (point support), and, for comparison, one with all nodes at the given angle constrained (line support). In all cases, axial supports were defined at the front surface edge node, with the same angular separation as the radial points. Only values for the CG mounting were tested. The lens mount for testing consisted of an aluminum backing plate and steel posts with rubber o-rings located to act through the CG plane of the optic. Axial (front surface) definition is provided by friction at the radial supports. **Figures 4** and **5** show the finite element prediction of the surface and the fringe analysis software (WYCO Wisp®) derived optical path difference for the lens on the 90° hard points. **Table 1** shows the comparison of the predicted P-V deformations with those derived from hand digitized interferometry, both as a function of separation angle (Θ). It has been noted that a 90° separation between supports is ideal, followed by 60°, and that a single support at 0° is superior to two points separated by 120°. Those conclusions are reaffirmed by these analyses, and, except in the 120° case, supported by the tests.

3.1.2. Band mount tests

The same input parameters were used for modeling the band support, with the exception of the boundary condition subroutine. For band supports, several variations were analyzed. Analyses were run for band widths of 1/4, 1/2, and full edge width of the optic. The 1/4 and 1/2 width band pressures were applied evenly spanning the CG of the lens, an option not possible with the full width band. Two types of axial supports were modeled. In the simplest case, 120° hard points provided the axial definition. In the second case, the front surface nodes, corresponding to the location of the band pressures, were fixed to simulate the axial friction effects of the actual bands. Two types of band supports were tested with the interferometer; a 6 mm (0.25 in.) wide plastic link chain, and a 0.5 mm (0.020 in.) thick stainless steel band lined with felt. The width and

location of the felt liner was varied to set the effective width of the band. The initial expectation was that the chain would provide a better approximation to the constant pressure assumption. However, the chain appeared to transfer excessive side loads into the optic, and did not perform as well as predicted. The felt appeared to provide more compliance in the axial direction, resulting in less than half the measured deformation of the chain band. **Table 2** shows the predicted and measured values for the P-V deformation of the band and model variations. **Figures 6** and 7 show the FEA predicted surface and the fringe analysis optical path difference (OPD) plots for the felt lined sling with the 3 point axial support.

The results of these analyses are open to interpretation. It is clear from the OPD plots that the nearly identical contours for the 90° hard point mount and the 1/4W band support are showing the actual figure of the optic, rather than the influence of the mounts. However, in both of those cases, the actual figures are significantly better than predicted by the models. Both the tests and the models are less than ideal. In the interferometric testing, results from several trials of the same mount varied as much as $\lambda/10$, depending on the care taken with the set-up. The best band test result was better than the three axial support model, but worse than the half axial ring model, suggesting that the transverse friction effects cannot be ignored, and that the simple, constant pressure band support model needs further development.

3.2. C2 lens blank tests

For the C2 lens blank analysis, the input file was run with the following parameters: Dia. = 816.2 mm (32.13 in.), R1 = R2 = 2.54E7 mm (1E6 in.), and central thickness 80.5 mm (3.169 in.). The FEA model used 790 nodes and 552 elements. The models were run with the optical axis vertical. Two analyses were run, one with three axial hard points spaced 120°

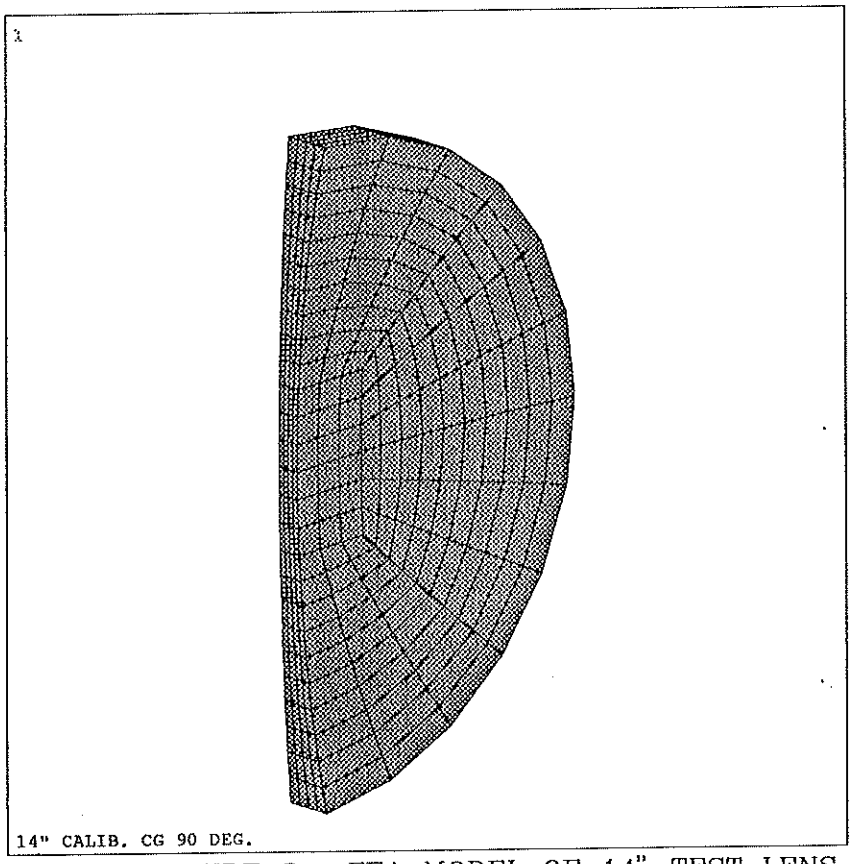

FIGURE 3. FEA MODEL OF 14" TEST LENS

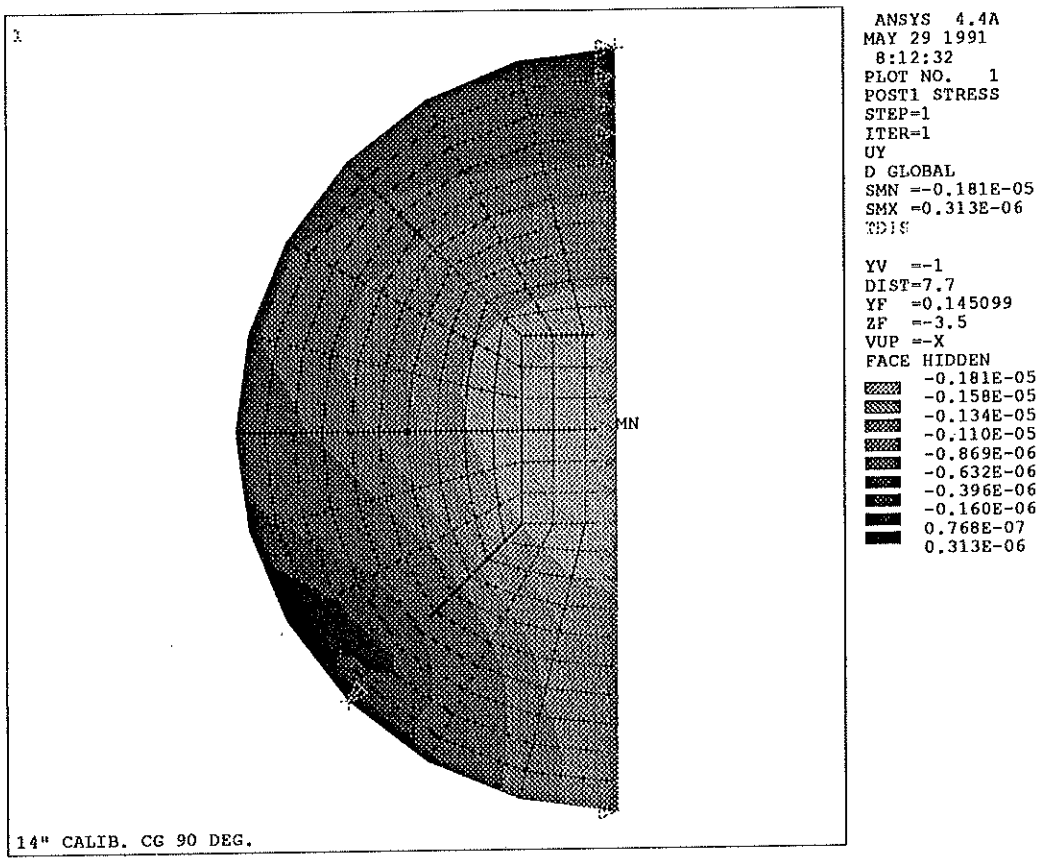

FIGURE 4. CONTOUR PLOT OF 14" LENS ON 90° RADIAL SUPPORT

Rms: 0.009 P-V: 0.057

OPD

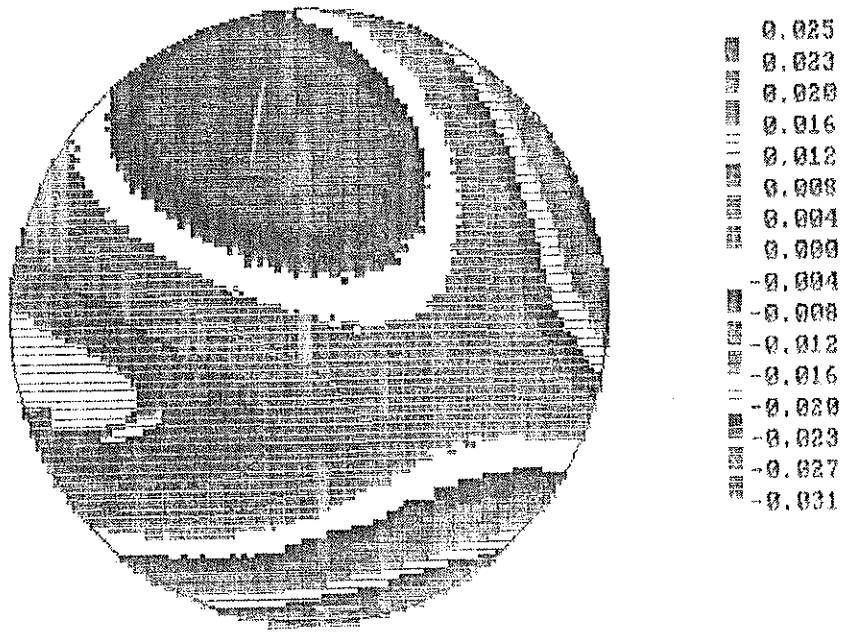

FIGURE 5. OPD PLOT OF 14" LENS ON 90° RADIAL SUPPORT

ANGLE (Θ)	NODES@(Θ)	P–V (μin)	λ CALC.	λ MEAS.
0°	ALL	7.7	0.30	
0°	CG	5.9	0.23	0.32
30°	ALL	6.6	0.26	
30°	CG	5.6	0.23	0.12
60°	ALL	5.2	0.20	
60°	CG	3.8	0.15	0.27
90°	ALL	3.5	0.14	
90°	CG	2.1	0.084	0.057
120°	ALL	11.4	0.45	
120°	CG	9.9	0.39	0.12

TABLE 1. DEFORMATION OF 14" LENS IN V–MOUNTS

around the circumference, and one with an idealized ring mount, with all nodes around the circumference of the optic constrained in the axial direction. The test fixturing for the hard point mount consisted of an aluminum pallet with three 12.7 mm (0.5 in.) nylon discs spaced 120° apart around the edge of the blank. The fixture for the ring mount used the same pallet, and a 12.7 mm (0.5 in.) ring of soft foam supporting the edge of the optic. The profilometer tests, unlike the interferometric tests, were very repeatable, and provided reassuring confirmation of the finite element predictions. The profilometer is accurate and repeatable to about 1 μin. **Figures 8** and **9** show the FEA predicted deformation across the diameter plotted with data measured on the Lick Observatory Anorad Profilometer, for the two support cases. The peaks and valleys in the profilometer data are the surface irregularities from the rough ground surface of the blank. The curve is a least squares fit to the data. In both of these tests, the predicted values agreed with the measured values within 1%. It is interesting to note that for the ring support, the theoretical maximum deflection under self loading, including bending and shear, can be calculated from formula found in Roark.[3] The predicted maximum deflection (shear and bending) for a flat disk of fused silica of the given size is 0.74 μm (29.7 μin.), or about 75% of the FEA predicted and measured value of 1 μm (40 μin.). For the three point support, the center deflection from bending (no shear) can be calculated using formulae from Timoshenko and Woinowsky-Krieger.[4] The calculated center deflection in this case is 1.67μm (66 μin.), or about 84% of the FEA predicted and measured value of 2μm (79μin.). Theoretical values aside, the FEA predictions and measured values agree very well, suggesting that in this case, the model and boundary conditions are an excellent analog for the behavior of the blank.

4. ANALYSIS OF HIRES LENSES

With the results from the calibration testing completed, the analysis of the two large lenses proceeded. There are several important differences between the calibration and HIRES lenses. The large lenses are mounted with their optical axes tilted 10.3° off the horizontal, which passes forces of 18% of the weight of the part through the axial supports. Both lenses are more than twice the diameter of the test lens, and quite different in cross section. The desired performance for the lenses was λ/4 P-V deformation over the clear aperture. The goal of the analyses was to identify the simplest mount that would satisfy the optical specifications. Due in part to the indeterminate nature of the sling support, and the uncertainties found in sling modeling and testing, hard point mountings were the preferred support method. Discussion of the analyses starts with lens C1, and then proceeds to C2.

SLING	WIDTH	AXIAL SUPT.	CALC.(μin)	CALC.(λ)	MEAS.(λ)
CHAIN	1/4	3@120°	1.79	0.071	0.169
S.STL./FELT	1/4	3@120°	1.79	0.071	0.061
S.STL./FELT	1/4	1/2 RING	1.10	0.043	0.061
S.STL./FELT	1/2	3@120°	1.79	0.071	
S.STL./FELT	FULL	3@120°	10.00	0.395	0.538

TABLE 2. DEFORMATION OF 14" LENS IN BAND MOUNTS

4.1. Meniscus lens C1

The standard input routine was run with the following parameters: Dia. = 769.6 mm (30.3 in.), R1 = 723.9 mm (28.5 in.), R2 = 1590 mm (62.6 in.), and thickness = 25.4 mm (1.0 in.). The preliminary models were run with 948 nodes and 690 elements, and increased in the final models to 1455 nodes and 1056 elements. The larger models were more desirable for increased accuracy around the support points, but required about thirty minutes to run, as opposed to fifteen minutes for the smaller models. The large models contained about 4200 degrees of freedom (DOF), and generated a solver rms wavefront of 239.

Results from the calibration analyses suggested that the ideal band support should provide the best radial mounting, and the ideal ring, the best axial mount. This set of supports was analyzed first to provide a comparison baseline for simpler and less idealized cases. The initial 1/4–width band and 12 point axial ring analyses predicted a P-V surface of 0.112 μm (4.5μin.), or about λ/5.6 in HeNe laser light, which was well within the desired tolerance. Then a variety of hard point supports were analyzed, starting with 2–point radial and 3–point axial supports, and gradually adding multiple, whiffled mounts. The simplest 2–point/3–point mount gave a λ/3 surface, which was surprisingly good, but not acceptable. By splitting the radial supports into two points spanning the CG at the two 90° locations, the surface improved to λ/4.18, slightly better than the desired value. However, it was desirable to have a surface margin of safety of at least 10% to 20%. Several variations on whiffled radial supports (one into two, two into four) were investigated, but no combination of radial hard points and 3 axial supports provided a surface better than the λ/4.18 of the previous model. Splitting the axial supports into three pairs, 45° apart on 120° centers, and using two CG points at eight radial locations from 45° to 90° apart, provided a P-V surface of λ/5.5. A simpler variation on this arrangement, with four radial points 90° and 45° apart (**figure 10**), performed almost as well, at λ/5.3. **Table 3** shows a selection of support variations and the predicted surface for each. It is worth noting here that an arrangement of eight radial and six axial support points performed within five percent of the idealized case.

4.2. Biconvex lens C2

The standard input routine was run with the following parameters: Dia. = 816.3 mm (32.14 in.), R1 = 5559 mm (218.86 in.), R2 = 2212.6 mm (87.11 in.), and center thickness = 72.9 mm (2.87 in.). As with C1, initial models were run with reduced node/element meshes, and later models were run with 1455 nodes and 1056 elements.

Idealized trials were again run to establish a baseline for comparison to subsequent simplified models. Unfortunately, even the idealized support, a radial band and axial ring, provided a surface of 0.6λ, two and a half times worse than required. Variations on the width of the sling and location of the axial ring failed to improve the surface quality beyond λ/2. It became clear that due to the very high aspect ratio and the 0.18W axial loading, simple passive supports would not be able to meet the specifications.

All the models following the initial baseline runs used additional force-couple inputs in an attempt to counter the deformations caused by gravity. Using formulae from Roark, and assuming a fixed edge and a 0.18W self–weight plate loading, a total reaction moment, due to flexure, of 10.3 N•m (91 in-lb) was calculated. This value provided the starting point for the

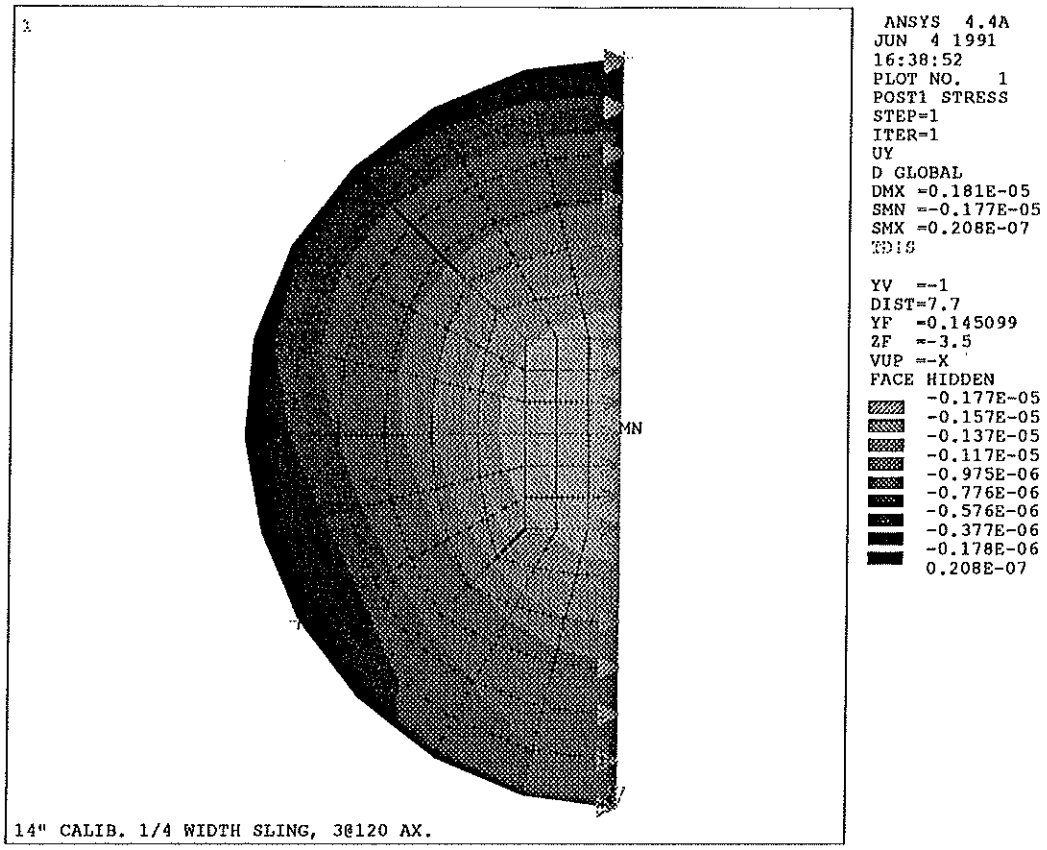

FIGURE 6. COUNTOUR PLOT OF 14" LENS IN SLING SUPPORT

Rms: 0.010 P-V: 0.061

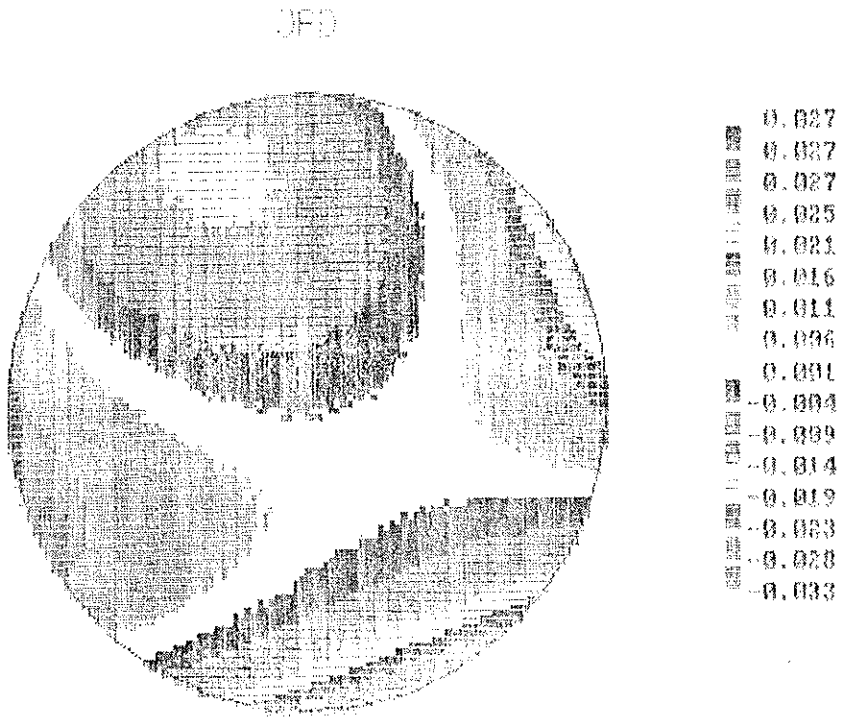

FIGURE 7. OPD PLOT OF 14" LENS IN SLING SUPPORT

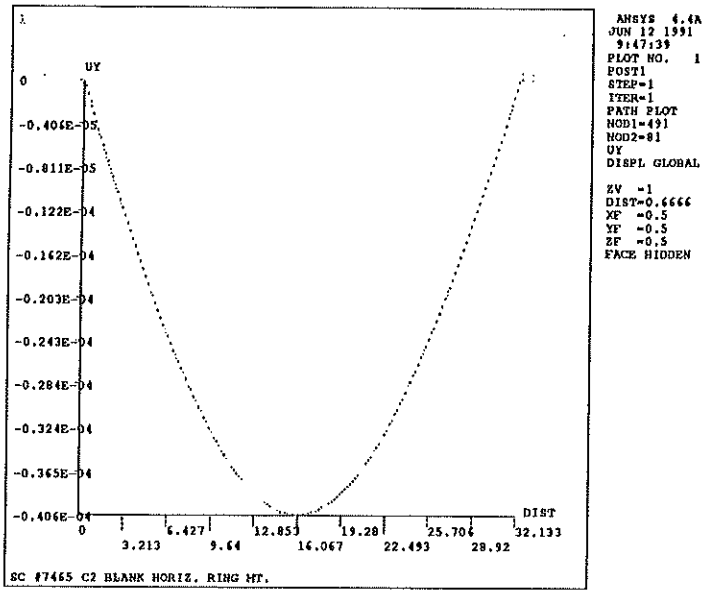

FIGURE 8.
C2 BLANK FEA PREDICTION

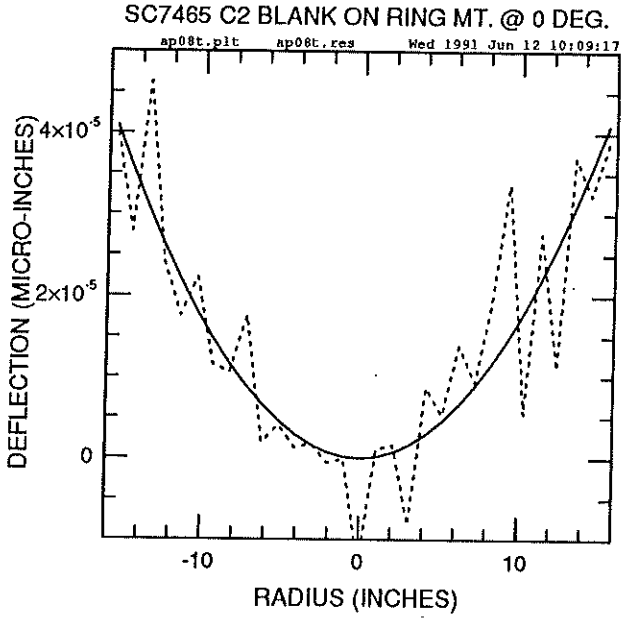

FIGURE 9.
C2 BLANK PROFILOMETER DATA

reforming moment loads on the lens. The first variations on the static deformation mount used a band support and axial hard points, in addition to positive and negative radial forces at the edge of the lens to create the compensating moment. However, the narrow edge width required large forces to create modest torque values. No combination of edge supports and various radially applied moments was found to provide better than a one-wave surface.

The next approach was to apply the force couples in the axial direction. Using the band radial support and the previous moment values as a starting point, twelve points around the back edge of the half model were fixed, and twelve forces were applied on the front surface on a circle 1 in. in from the edge, on 15° centers. Multiple load cases were run for each analysis to determine the optimum point forces for each support variant. This approach, using an optimum force of 1363 g. (3 lb.), produced a surface with $\lambda/6.3$ P-V deformation. This provided a new baseline from which to explore simpler hard point radial mounts. **Table 4** shows some of the axial and radial hard point combinations which were examined. It was desirable to find a mounting configuration similar to that of C1 in order to use a common cell and hardware for both. Unfortunately, no six point axial support, regardless of the radial support, provided better than a $\lambda/3.7$ surface. The simplest acceptable support (half model) used 6 axial defining points and 6 axial forces on 30° centers, and a two–into–four whiffletree split over the CG for a total of eight radial support points. The mount provided a P-V surface of $\lambda/5.2$ (**figure 11**), comfortably meeting the requirement. The problem of stress birefringence arises whenever forces are applied to an optic. In this case, the maximum stress level never exceeds 50 psi, well below the commonly accepted limit of 500 psi.[5]

5. CONCLUSIONS

The purpose of these analyses was to find the simplest acceptable quarter-wave supports for the lenses, and that objective has been met. Several additional conclusions can be drawn from this work. The analyses and tests described here show that commercially available finite element modeling codes can be an extremely powerful and accurate tool for the analysis of large lenses. This work builds upon previous analyses of large reflecting optics, and not surprisingly, some of the same methods and mounts can be adapted for use on large lenses. The superiority of the 90° v-mount is confirmed. Large, stationary lenses with high aspect ratios can be simply supported as long as the optical requirements are not much greater than $\lambda/4$ P-V for surface deformation. For more stringent applications, the statically deforming lens mount, although not yet proven, may provide a viable alternative for mounting large, thin section lenses. Areas for future work include more generalized analyses for various lens configurations and orientation angles, and an interface to optical design and analysis packages for exchange of geometry and deformed surfaces.

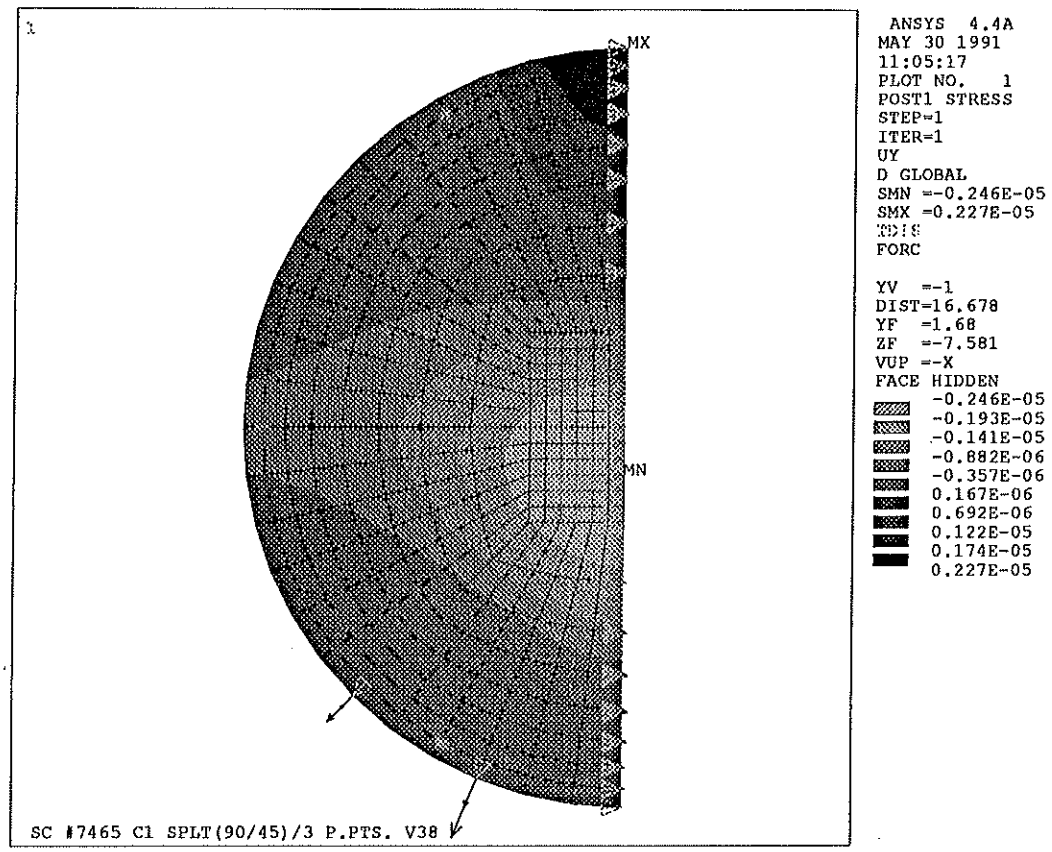

FIGURE 10. COUNTOUR PLOT OF LENS C1

RUN	AXIAL SUPT.	AXIAL SUPT.	CALC.(μin)	CALC.(λ)
V1	12 POINT RING	1/4W SLNG	4.48	0.177
V2	3@120	2@90	8.66	0.339
V3	3@120	4@90	6.00	0.237
V4	3@120	6@90	5.94	0.233
V5	3 X 2@45 ON 120' CENT.	4@90 4@75 4@60 4@45	4.57	0.181
V6	6@60	4@90 4@45	4.73	0.187
V7	6@60	4@90 4@75 4@60 4@45	4.78	0.189
V8	12@30	4@90 4@60	4.27	0.168
V9	12@30	4@90 4@60	4.44	0.175

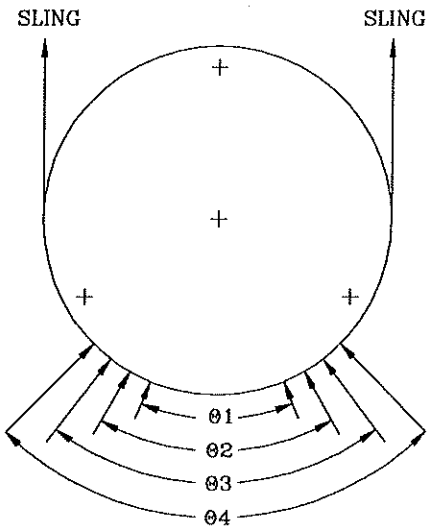

TABLE 3. SUPPORT VARIATIONS FOR LENS C1

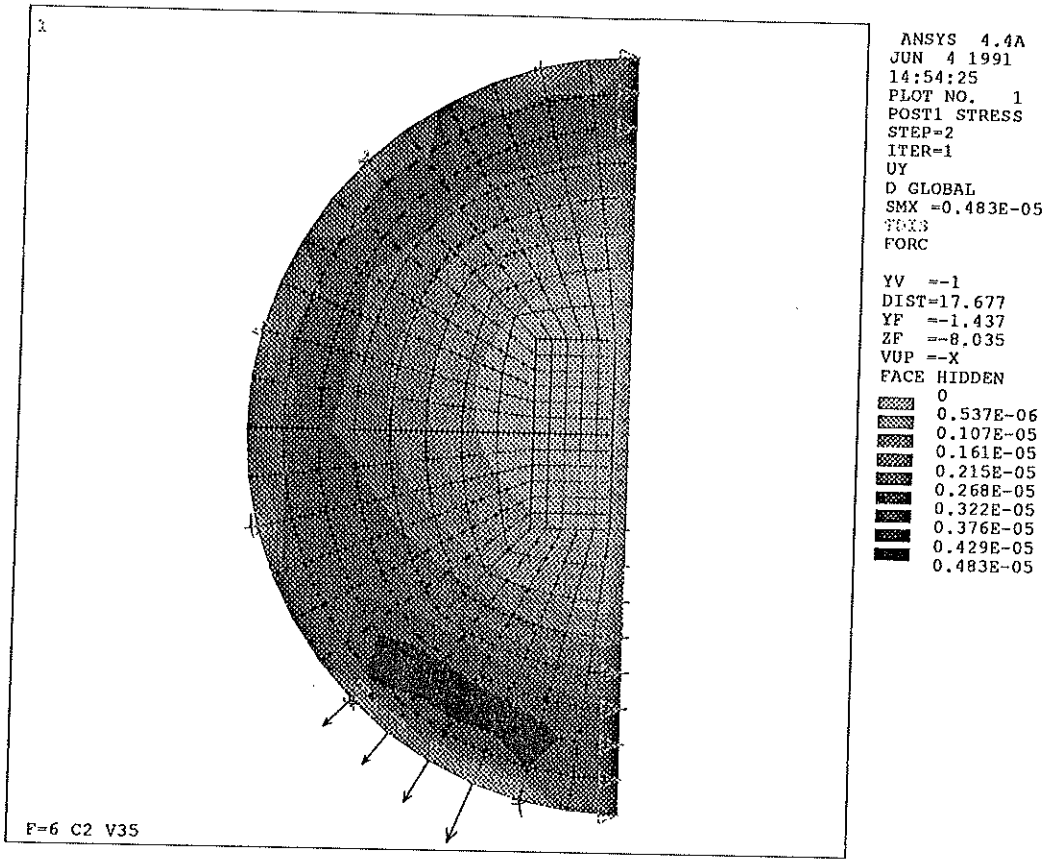

FIGURE 11. CONTOUR PLOT OF LENS C2

RUN	AXIAL SUPT.	RADIAL SUPT.	FORCE(lbs)	CALC.(μin)	CALC.(λ)
V1	3@120	2@90	–	38.5	1.52
V2	RING	2@90	–	16.6	0.656
V3	RING	1/4W SLNG	–	15.7	0.621
V4	RING	1/2W SLNG	–	12.4	0.490
V5	RING	1/2W SLNG	3	4.04	0.159
V6	6@60	4@90 4@45	5.5	6.63	0.262
V7	12@30	4@90 4@75 4@60 4@45	6	4.83	0.191
V8	12@30	6@90 6@75 6@60 6@45	6.5	4.97	0.196

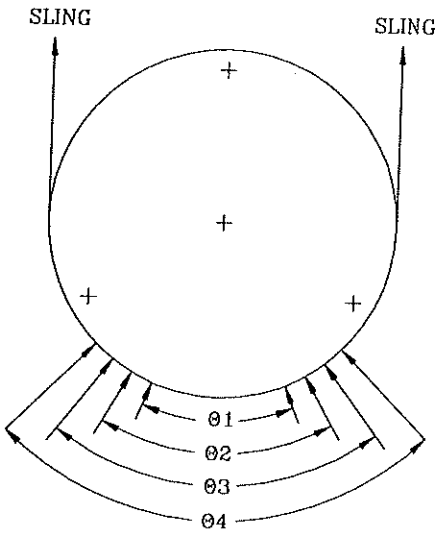

TABLE 4. SUPPORT VARIATIONS FOR LENS C2

6. ACKNOWLEDGMENTS

This work was performed as a part of development and design of the Keck Telescope High Resolution Spectrograph, and funded by the California Association of Research in Astronomy. Many people provided support in the course of this work. The author wishes to thank the following people for their assistance: Mark Rodamaker of MCR Associates, Sunnyvale, Ca., ANSYS® distributor, for initial design of the parametric input routine and patient phone support; Gerard Pardeilhan, of the Lick Optical Lab, for performing the interferometric and profilometric testing as described; and to Steve Allen, of Lick Observatory, for help with data analysis and the Mongo interactive graphics program.

7. REFERENCES

1. A. J. Malvick, "Theoretical Elastic Deformations of the Steward Observatory 230–cm and the Optical Sciences Center 154–cm Mirrors," Applied Optics, Vol. 11, No. 3, pp. 579–585, March, 1972.

2. Gerhard Schwesinger, "Optical Effect of Flexure in Vertically Mounted Precision Mirrors," JOSA, Vol. 44, No. 5, pp. 417–424, May, 1954.

3. R. J. Rourk and W. C. Young, Formulas for Stress and Strain, 5th. Ed., Chap. 10, McGraw-Hill, New York, 1975.

4. S. Timoshenko and S. Woinowsky-Krieger, Theory of Plates and Shells, 2nd. Ed., Chap. 9, McGraw-Hill, New York, 1968.

5. P. R. Yoder, Opto-Mechanical Systems Design, Chap. 4, Marcel Dekker, Inc., New York, 1986.